Journal of the European Ceramic Society **18** (1998) 1621–1628

PII: S0955-2219(98)00028-4
0955-2219/98/$—see front matter

Dielectric Relaxation Behaviour of Bi:$SrTiO_3$: II. Influence of Heat Treatment on Dielectric Properties

Yu Zhi, Ang Chen*, P. M. Vilarinho, P. Q. Mantas and J. L. Baptista†

Department of Ceramics and Glass Engineering, University of Aveiro, 3800 Aveiro, Portugal

(Received 1 July 1997; accepted 2 February 1998)

Abstract

The study of the dielectric properties of $(Sr_{1-1.5x}Bi_x)TiO_3$ *ceramics in a range of temperatures and at several frequencies showed that a set of permittivity peaks situated around 200–300 K had frequency dispersion behaviour. These peaks were shifted to higher temperatures when the Bi content increased in the solid solution. The activation energy calculated for the relaxation varied between 0·32–0·49 eV. This set of permittivity peaks vanished if the samples were annealed in air or oxygen and their permittivity maximum was increased by annealing in nitrogen. The temperature dependence of resistance was also measured. The origin of dielectric behaviour is discussed in the present paper.* © *1998 Elsevier Science Limited. All rights reserved*

1 Introduction

Skanavi *et al.*[1–3] reported almost 40 years ago, that the solid solutions of $(1-x)SrTiO_3$–$xBi_{2/3}TiO_3$ show dielectric permittivity peaks at low temperatures and attributed this behaviour to Ti ion hopping.[2] Smolenskii *et al.*[4] however considered it to be due to a ferroelectric mechanism.

Looking at several solid solutions in the same system, the present authors found that, besides the previously reported low temperature peaks,[1–3,5,6] other sets of permittivity peaks are also present and show dispersion behaviour. For example, the composition with $x = 0{\cdot}0267$, besides the peak around 100 K (1 kHz) which was reported by Skanavi,[1–3] exhibits another set of permittivity peaks around 210 K (the exact peak temperature depending on the measuring frequency). A similar type of behaviour has been described for La doped $SrTiO_3$, where several dielectric peaks were reported, first by Tien and Cross,[7] at 170 and 470 K, and more recently, another one around 70 K by Iguchi and Lee,[8] who also found two individual (partially overlapped) peaks in $(Sr_{1-3x/2}La_x)(Mn_yTi_{1-y})O_3$ ceramics. Moreover when a series of strontium titanate ceramics containing rare-earth ions were systematically studied, it was found that the activation energy for relaxation ranged from 0·20 to 0·45 eV and the activation energy for conduction ranged from 0·65 to 0·80 eV for different rare-earth ions and various concentrations.[9]

The above work indicated that when $SrTiO_3$ is doped with Bi or La (or other rare-earth elements) several polarisation phenomena, in different temperature ranges, could take place.

It seemed therefore interesting to have a deeper look into the origin of polarisation and relaxation in the Bi doped $SrTiO_3$ system. The present paper is mainly concerned with the study of the set of permittivity peaks around 200–300 K and the influence of heat treatment in the solid solution $(Sr_{1-1.5x}Bi_x)TiO_3$ ceramics with the Bi contents in the range of 0·0133–0·133.

2 Experimental Procedure

The ceramic samples were prepared by solid state reaction. Raw materials ($SrCO_3$, Bi_2O_3 and TiO_2) were weighed according to the composition $(Sr_{1-1.5x}Bi_x)TiO_3$, where $x = 0{\cdot}0133$, 0·0267, 0·04, 0·0533, 0·08, 0·10 and 0·133, respectively, and the samples obtained as described previously.[5]

The complex–impedance of the $(Sr_{1-1.5x}Bi_x)TiO_3$ samples was measured with an HP3330 LCZ Meter and a Solartron 1260 Impedance Gain-Phase Analyser in the frequency range from 1 Hz to

*Permanent address: Department of Physics, Zhejiang University, Hangzhou 310027, People's Republic of China.
†To whom correspondence should be addressed. Fax: 00351 34 25300.

1 MHz. The dc resistance of the samples was measured with a Keithley-617 Programmable Electrometer.

The temperature dependence of dielectric properties and dc resistance was measured in a cryogenic system from 60 to 300 K, while the temperature of the samples was changing at a rate of 1°C min^{-1}. Data were taken every 2·5°C.

In addition, sintered samples, with $x = 0{\cdot}0133$, 0·0267, 0·04, 0·0533 and 0·08, were annealed under 1 atm of either oxygen or air at 1000–1100°C for 40–100 h and furnace-cooled. The ceramic samples with $x = 0{\cdot}0533$ and 0·10 were annealed under 1 atm of nitrogen at 1000°C for 88 h. After that, the temperature dependence of capacitance as well as the resistance of each annealed sample were measured again.

X-ray powder diffraction (XRD), scanning electronic microscopy (SEM) and the energy dispersion spectrum (EDS) were used to characterise the phase structure and to analyse the chemical composition.

3 Experimental Results

3.1 Structure, density and resistivity

XRD results show that all the ceramic compositions $(Sr_{1-1.5x}Bi_x)TiO_3$ ($x \leq 0{\cdot}133$) have a cubic structure with a gradual increase of the lattice parameter with increasing Bi, in accordance with previous work.[5,10] SEM observations show that the grain size is 2–4 μm without systematic variation with the increase in the Bi concentration. EDS results showed that the Bi content of the samples is in agreement with the nominal composition within the experimental error. Neither obvious variation in the lattice parameter nor grain growth of the samples was found after heat treatment. The sintering temperature (T_s), relative density (D_r) and dc resistivity (ρ) of the $(Sr_{1-1.5x}Bi_x)TiO_3$ samples are listed in Table 1. For the as-sintered samples, the resistivity is about $1\text{-}6\times10^{10}\,\Omega\bullet$cm when $x \leq 0{\cdot}08$, and $1\text{–}7\times10^{11}\,\Omega\bullet$cm when $x = 0{\cdot}10$ and 0·133.

Table 1. The sintering temperature (T_s), relative density (D_r) and dc resistivity (ρ) at room temperature for the as-sintered, O_2 annealed, and N_2 annealed samples of $(Sr_{1-1.5x}Bi_x)TiO_3$ ceramics

X	T_s (°C)	D_r (%)	ρ (Ω·cm) (as-sintered)	ρ (Ω·cm) (O_2-annealed)	ρ (Ω·cm) (N_2-annealed)
0·0133	1380	92	$2{\cdot}7\times10^{10}$	$2{\cdot}6\times10^{11}$	—
0·0267	1380	96	$1{\cdot}2\times10^{10}$	$2{\cdot}3\times10^{11}$	—
0·04	1380	95	$5{\cdot}3\times10^{10}$	$4{\cdot}0\times10^{11}$	—
0·0533	1350	91	$5{\cdot}8\times10^{10}$	$7{\cdot}9\times10^{11}$	$2{\cdot}4\times10^{9}$
0·08	1350	91	$1{\cdot}1\times10^{10}$	$6{\cdot}0\times10^{11}$	—
0·10	1300	90	$6{\cdot}5\times10^{11}$	—	$6{\cdot}8\times10^{8}$
0·133	1300	91	$1{\cdot}3\times10^{11}$	—	—

3.2 Dielectric behaviour of as-sintered samples

The temperature dependence of the real part of the complex-permittivity (ε') for $x = 0{\cdot}0133$, 0·0267, 0·04, 0·0533, 0·08, 0·10 and 0·133 at 1 kHz from 60 to 290 K is shown in Fig. 1. It is observed that there are two sets of peaks for $x \leq 0{\cdot}08$; one occurred at a low temperature (60–150 K), and the other occurred at higher temperature. The temperature range ΔT where the second set of permittivity peaks occurred for each composition is given in Table 2. For $x = 0{\cdot}10$ and 0·133, only one peak in the temperature range from 60 to 400 K, was observed.

For the lower Bi contents ($x = 0{\cdot}0133$ and 0·0267), the permittivity maximum of the second peak is much higher than that of the first one. As the Bi content increases ($x = 0{\cdot}0533$), the maximum of the second peak decreases. For $x = 0{\cdot}08$, the second peak is not obvious and for $x = 0{\cdot}10$ and 0·133, it cannot be seen (even if the temperature was raised up to 400 K). The real and imaginary parts of the complex-permittivity (ε' and ε'') as a function of temperature and frequency were measured between 60 and 290 K. Figure 2(a) only shows the results for the sample with $x = 0{\cdot}0533$ at frequencies 0·1, 1, 10 and 100 kHz, the others being similar. A broad ε' peak, with obvious frequency dispersion, together with a shift of the ε'' maximum to higher temperatures for higher frequencies can be observed.

The effect of the Bi content on the temperature of the permittivity maximum is shown in Fig. 3. The temperature of the permittivity maximum is increased with the Bi content, both for the first peak ($T_{max\,1}$) and for the second one ($T_{max\,2}$). From the tendency of the composition dependence of $T_{max\,1}$ and $T_{max\,2}$, it is reasonable to recognise that the peak for $x = 0{\cdot}10$ and 0·133 belongs to the first

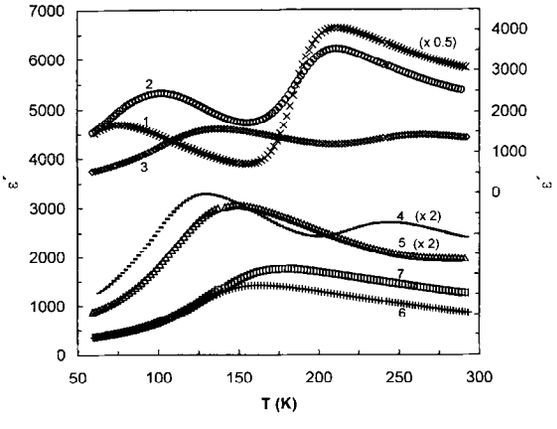

Fig. 1. Temperature dependence of ε' at 1 kHz for the as-sintered $(Sr_{1-1.5x}Bi_x)TiO_3$ ceramics with $x = 0{\cdot}0133$ (1), 0·0267 (2), 0·04 (3), 0·0533 (4), 0·08 (5), 0·10 (6) and 0·133 (7). (Notes: 4–7, the left scale; 1–3, the right scale; the label in brackets is the magnification scale).

Table 2. The activation energy for relaxation derived by fitting Cole–Cole plots, the temperature range ΔT, corresponding to the second set of peaks and some data of the activation energy for conduction of $(Sr_{1-1.5x}Bi_x)TiO_3$ ceramics

x	*0·0133 (as-sintered)*	*0·0267 (as-sintered)*	*0·04 (as-sintered)*	*0·0533 (as-sintered)*	*0·0533 (N_2-annealed)*	*0·08 (as-sintered)*
ΔT (K)	130–310	140–320	150–330	170–350	170–350	200–380
E_{relax2} (eV)	0·32	0·31	0·43	0·48	0·48	0·49
E_{cond2} (eV)	0·13	—	—	0·26	0·28	—

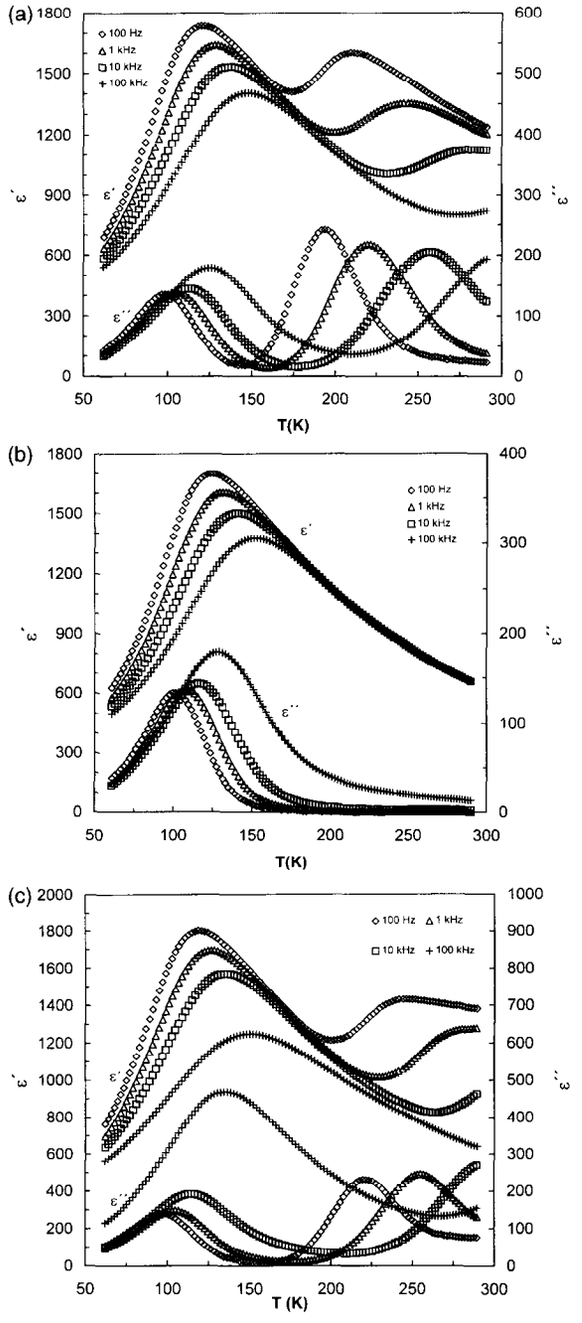

Fig. 2. Temperature dependence of ε' and ε'' for $(Sr_{1-1.5x}Bi_x)TiO_3$ ceramics with $x = 0{\cdot}0533$ at 100 Hz (◇), 1 kHz (△), 10 kHz (□) and 100 kHz (+): (a) as-sintered; (b) after annealing in oxygen; (c) after annealing in nitrogen.

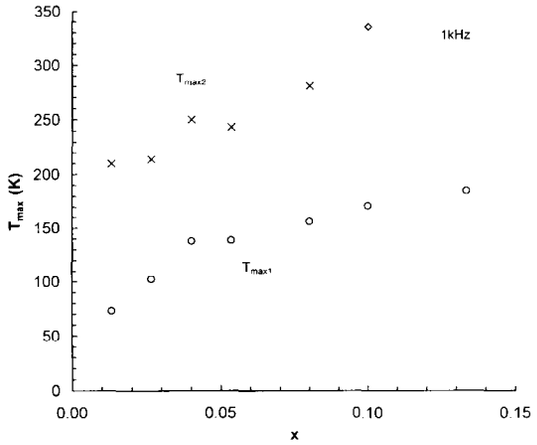

Fig. 3. Temperature of permittivity maximum (T_{max1} and T_{max2}) at 1 kHz versus Bi content for the as-sintered $(Sr_{1-1.5x}Bi_x)TiO_3$ ceramics, (◇) data from the sample with $x = 0{\cdot}1$ annealed in N_2.

set. The second set of peaks only occurred in the low Bi content samples ($x \leq 0{\cdot}08$), as shown in Fig. 1.

The frequency dependence of the real (ε') and imaginary parts (ε'') of the complex-permittivity for $x = 0{\cdot}0267$, and 0·04 at room temperature is shown in Fig. 4. Dielectric relaxation occurred for both samples in this frequency range and, correspondingly, the ε'' peak occurred at $6{\cdot}0\times10^5$ Hz and $1{\cdot}3\times10^4$ Hz, for $x = 0{\cdot}0267$ and 0·04, respectively. From the simple Debye relaxation model, $\omega\tau = 1$ at the ε'' peak, the relaxation time at room temperature was calculated, being $1{\cdot}7\times10^{-6}$ s for $x = 0{\cdot}0267$ and $7{\cdot}7\times10^{-5}$ s for $x = 0{\cdot}04$. For $x \leq 0{\cdot}08$, all the samples have a similar profile of frequency dependence. Moreover, the ε'' peak is shifted to lower frequencies, with the increase in bismuth content; this is in agreement with the increase of T_{max2} with the increase in Bi content.

For the second set of peaks, we choose the sample with $x = 0{\cdot}0533$ to plot the curve of the real part versus the imaginary part of complex-permittivity, i.e. the Cole–Cole plot. As shown in Fig. 5, the data points fit well into a semicircular arc with the centre lying underneath the abscissa. The complex-permittivity can be empirically described by the equation:[11]

$$\varepsilon^* = \varepsilon\infty + (\varepsilon_0 - \varepsilon\infty)/[1 + (i\omega\tau)^{\beta}] \qquad (1)$$

where ε_0 is the static permittivity, $\varepsilon\infty$ is the permittivity at high frequency, ω is the angular frequency, τ is the mean relaxation time, and $\beta = 1 - \alpha$, where α is the angle of the semicircular arc. By fitting this arc with the least square

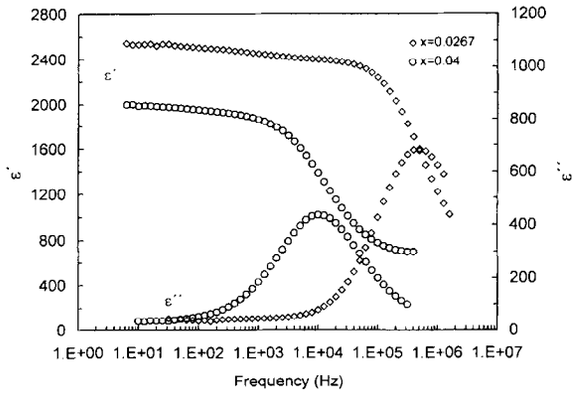

Fig. 4. Frequency dependence of ε' and ε'' for the as-sintered $(Sr_{1-1.5x}Bi_x)TiO_3$ ceramics with $x = 0.0267$ and 0.04 at room temperature.

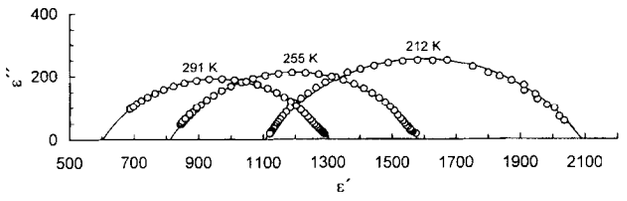

Fig. 5. Cole–Cole plot (ε' versus ε'') of the as-sintered $(Sr_{1-1.5x}Bi_x)TiO_3$ ceramics with $x = 0.0533$ at 212, 255 and 291 K (Dots: experimental data; circular arcs: fitting curves).

approach (Fig. 5), $\varepsilon_0 = 1297$, $\varepsilon\infty = 603$, and $\beta = 0.64$ at 291 K can be obtained. In the temperature interval 200–300 K, β is in the range of 0.61–0.65.

The real and imaginary parts of the permittivity can be rewritten from eqn (1) in the following way:

$$\varepsilon' = \varepsilon\infty + (\Delta\varepsilon'/2)\{1 - \sinh(\beta z)/[\cosh(\beta z) + \cos(\beta\pi/2)]\} \quad (2)$$

$$\varepsilon'' = (\Delta\varepsilon'/2)\sin(\beta\pi/2)/[\cosh(\beta z) + \cos(\beta\pi/2)] \quad (3)$$

where $z = \ln(\omega\tau)$ and $\Delta\varepsilon' = \varepsilon_0 - \varepsilon\infty$.

If the dielectric relaxation is related to a thermally activated process, the relaxation time will obey the following relation:

$$\tau = \tau_0 \exp[E_{relax2}/(k_B T)] \quad (4)$$

where τ_0 is the relaxation time at infinite temperature, E_{relax2} the activation energy for relaxation, k_B the Boltzmann's constant, and T the temperature.

Using eqns (2) and (3), the relaxation time was calculated from 200 to 300 K for $x = 0.0533$. The relaxation time τ against the reciprocal of the absolute temperature ($1/T$) at 0.1, 1, 10 and 100 kHz is shown in Fig. 6. The relation between $\log\tau$ and $1/T$ is linear and this linear relation gave an activation energy for the relaxation process, $E_{relax2} = 0.48$ eV. Similar fitting was done for the samples with $x = 0.0133$, 0.0267, 0.04, 0.0533 and 0.08. The activation energies are in the range of 0.32–0.49 eV for the as-sintered samples with $x \leq 0.08$ and are summarised in Table 2.

3.3 Dielectric behaviour of annealed samples

The colour of the as-sintered samples depended on the Bi content. For low x values, the colour was dark grey, while for high x values, the colour was increasingly lighter. Dark colour in Ti based ceramics is usually related to a reduced state of the material.[12] Since the second set of permittivity peaks is vanished with the increase in Bi content as $x \geq 0.10$, it is reasonable to expect some sort of correlation between the two phenomena, both being probably caused by an oxidation process.

In order to confirm this idea, the samples were annealed under controlled atmospheres.

3.3.1 Annealing in oxygen and air

Figure 7 shows the effect of annealing in oxygen and air on the dielectric characteristics of the $x = 0.0133$ sample. It can be seen that, as expected, the intensity of the second set of peaks is decreased with the increase in the annealing time and finally disappeared. It is a very slow process, probably indicating that it is related to the bulk of the grains, i.e. the defects being oxidised are homogeneously distributed in the material. After annealing, the sample has a light colour and its resistivity increases (Table 1). The temperature dependence of the real and imaginary parts of the complex-permittivity for the sample with $x = 0.0533$ after annealed in oxygen is shown in Fig. 2(b). It can be seen that the second set of permittivity peaks vanished during oxygen annealing. These phenomena were also observed for the other samples that exhibit the second set of permittivity peaks.

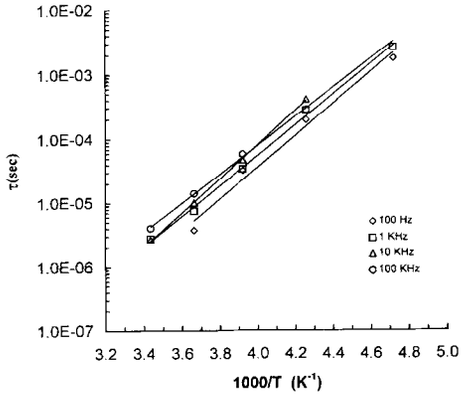

Fig. 6. Relaxation time τ versus $1/T$ curve for the as-sintered $(Sr_{1-1.5x}Bi_x)TiO_3$ ceramics with $x = 0.0533$ at 100 Hz, 1, 10 and 100 kHz (Dots: experimental data; lines: fitting curves).

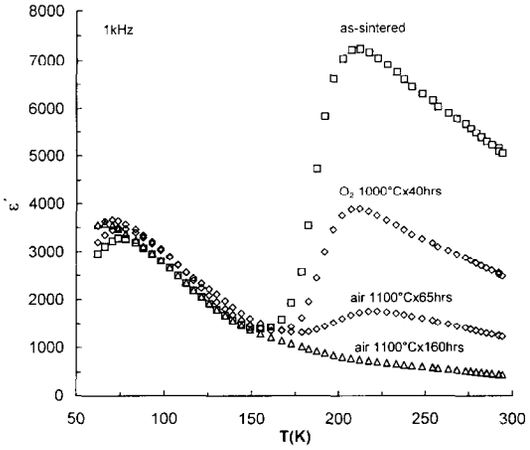

Fig. 7. Temperature dependence of ε' under different annealing conditions (atmosphere, temperature and time) for $(Sr_{1-1.5x}Bi_x)TiO_3$ ceramics with $x = 0.0133$.

3.3.2 Annealing in nitrogen

As indicated above for the samples with Bi content $0.0133 \leq x \leq 0.08$, the second set of peaks disappeared after annealing in oxygen or air at 1 atm. This indicates that the second set of peaks is probably related to the oxygen content. In order to confirm this, the samples with $x = 0.08$ and 0.10 were annealed at 1000°C for 88 h under 1 atm of nitrogen. The temperature dependence of permittivity and dissipation factor at 100 Hz, 1, 10 and 100 kHz for the sample with $x = 0.0533$ after N_2 annealing is shown in Fig. 2(c). Figure 8(a) and (b) compares the temperature dependence of permittivity and dissipation factor at 100 Hz, 1, 10 and 100 kHz for the as-sintered and N_2 annealed sample with $x = 0.10$. The influence of nitrogen atmosphere treatment on the dielectric characteristics of the samples can be clearly seen. The intensity of the second ε'' peak is further increased for $x = 0.0533$ and one more permittivity peak was created for $x = 0.10$ after nitrogen annealing. The activation energy for relaxation for the N_2-annealed sample with $x = 0.0533$ is the same as the as-sintered one, which is also shown in Table 2.

3.4 Temperature dependence of conductivity

The temperature dependence of the dc conductivity (σ) of the sample with $x = 0.0533$ both as-sintered and annealed in nitrogen was measured. The curve of σ versus the inverse absolute temperature ($1/T$) is shown in Fig. 9. The conductivity can be expressed by the following equation:

$$\sigma = \sigma_0 \exp[E_{\text{cond}}/(k_B T)] \qquad (5)$$

where σ_0 is the pre-exponential term, E_{cond} is the conduction activation energy and k_B and T are as defined before.

The data for the sample after annealing under N_2, can be fitted by two straight lines. The activation energies of 0.03 and 0.23 eV were calculated from 25 to 170 K and from 170 to 300 K, respectively.

For the as-sintered sample, similar behaviour was obtained. The transition temperature is also around 170 K, and the activation energy above this temperature is 0.26 eV.

Comparing Fig. 9 with Fig. 2(a) and (c), it is interesting to note that the transition temperature for the different slopes of the conductivity against $1/T$ curve, corresponding to the different types of conduction mechanisms, coincides with the transition temperature for the two permittivity peaks. In the temperature range where the second set of peaks occurred, the activation energy for conduction of the as-sintered and nitrogen annealed samples is 0.26 and 0.28 eV, respectively, as shown in Table 2. These two values are similar within the experimental error. The activation energy for conduction is smaller than the one for the dielectric relaxation ($E_{\text{relax2}} = 0.48$ eV). Furthermore, for the sample with $x = 0.0133$, the activation energy for dc conduction measured is 0.13 eV in the temperature interval where the second set of peaks occurred.

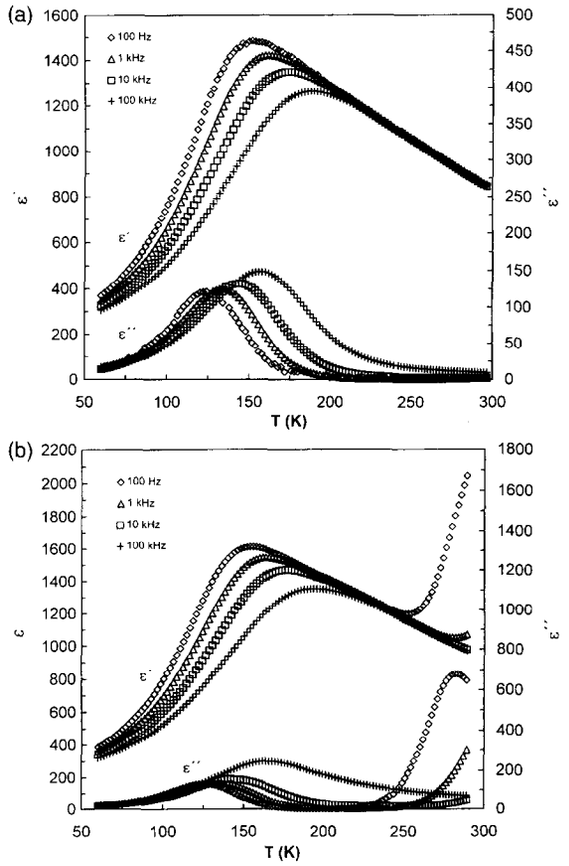

Fig. 8. Temperature dependence of real and imaginary parts of complex-permittivity (ε' and ε'') for $(Sr_{1-1.5x}Bi_x)TiO_3$ ceramics with $x = 0.10$ at 100 Hz (◇), 1 (△), 10 (□) and 100 kHz (+): (a) as-sintered; (b) after annealing in nitrogen.

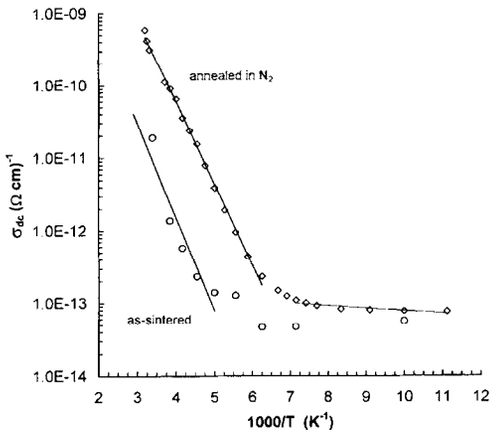

Fig. 9. dc Conductivity (σ_{dc}) versus $1/T$ curve for the as-sintered (○) and nitrogen annealed (◇) $(Sr_{1-1.5x}Bi_x)TiO_3$ ceramics with $x = 0.0533$.

4 Discussion

4.1 Dielectric properties

The above experimental results on the second set of peaks can be summarised as follows:

1. These peaks were observed for the low Bi content samples ($x \leq 0.08$) and the permittivity maximum decreased with the increase in Bi content. They were not present in the high Bi content samples ($x = 0.10$ and 0.133).
2. The peaks could be eliminated from the samples with low Bi content ($x \leq 0.08$) by annealing in oxygen or air, and the elimination of the peaks was gradual, i.e. the permittivity maximum decreased gradually with the increase in annealing time. The peaks could be enhanced or created by annealing in nitrogen atmosphere.
3. With the increase in Bi content, T_{max2} rises and the activation energy E_{relax2} for relaxation rises simultaneously. The frequency of the imaginary permittivity peak ε''_m at room temperature decreased with the increase in Bi content, i.e. the relaxation time of the second set of peaks increased.
4. For the samples with $x = 0.0133$ and 0.0533, the activation energy for dielectric relaxation is higher than the activation energy for conduction in the temperature range where the second set of permittivity peaks occur.

The experimental results above indicate that this set of peaks is influenced by an oxidation ↔ reduction process which is related to the defect structure of the $(Sr_{1-1.5x}Bi_x)TiO_3$ solid solution.

4.2 Defect structure

In Bi doped $SrTiO_3$, because trivalent Bi^{3+} ions replaced divalent Sr^{2+} ions, some charge compensation is needed to maintain electro-neutrality. Earlier work of Skanavi[1] showed that the solid solutions can be divided into two types differing in the charge compensation mechanisms. This was confirmed by further studies of the dielectric properties and defect structure in $(Sr_{1-x'}Bi_{2x'/3})TiO_3$ solid solutions[13,14] one with low Bi contents ($x' = \leq\sim 0.11$) and the other with high Bi contents ($x' >\sim 0.11$). The transition of the Bi content is, considering the present data, for $x = 0.08$, since the second permittivity peak is still present for $x = 2x'/3 = 0.08$ and is absent for $x > 0.08$.

Previous work[12] indicated that in donor-doped $SrTiO_3$, as the donor concentration was greater than 0.2 mol%, the cation vacancy compensation was predominant (and the electron compensation could be neglected). In the present $(Sr_{1-1.5x}Bi_{x)TiO_3}$ solid solutions with x from 0.0133 to 0.133, the electrical unbalance caused by the trivalent Bi ions substituting the divalent Sr ions can be compensated by the creation of strontium vacancies, considering the SrO sublattice, i.e.

$$Bi_2O_3 \xrightarrow{3SrO} 2Bi^{\bullet}_{Sr} + 3O^{x}_{0} + V''_{Sr} \qquad (6)$$

where the Kröger–Vink notation of defects is adopted. $V_{Sr''}$ represents the strontium vacancy carrying two excess negative charges.

On the other hand, many studies on non-stoichiometric, donor-doped and acceptor-doped strontium titanate have shown that oxygen vacancies are easily created by loss of oxygen from the crystal lattice at low oxygen partial pressure or high temperatures[12,15–20] according to

$$O^{x}_{o} \rightarrow V^{\bullet}_{o} + e' + 1/2\ O_2 \qquad (7a)$$

or

$$O^{x}_{o} \rightarrow V^{\bullet\bullet}_{o} + 2e' + 1/2\ O_2 \qquad (7b)$$

where $V^{\bullet}_{o}$ and $V^{\bullet\bullet}_{o}$ represent the oxygen vacancy carrying one and two excess positive charges, respectively.

Although the trivalent Bi could be mainly compensated by strontium vacancies as indicated above, it is possible that some loss of oxygen has occurred in the low Bi content region during high temperature sintering (Ts$\geq$1350°C). So reaction (7a) or (7b) would occur, i.e. weakly bonded electrons could be created at the high sintering temperatures. These samples show dark grey colour.

It seems therefore that in the low Bi content region ($x \leq 0.08$), the charge compensation mechanisms from eqns (6) and (7) could coexist. With the increase of Bi content and the decrease in the sintering temperature ($x = 0.10$ and 0.133), the

oxygen vacancy concentration decreases and the cation vacancy (V_{Sr}) compensation becomes predominant as described by eqn (6).

4.3 Polarisation mechanism

The possibility of the contact between the electrodes and samples influencing the dielectric properties can be excluded, because the dielectric behaviour was independent of the thickness of the samples as well as of the type of the electrodes adopted.

As mentioned above, the second set of permittivity peaks is related to the oxidation ↔ reduction process, i.e. to weakly bonded electrons. The defects $V_O^{\bullet}$ and Ti'_{Ti} (Ti^{3+}) with weakly bonded electrons can be considered. Two possibilities for the polarisation mechanism leading to the second set of permittivity peaks, both correlated with weakly bonded electrons in shallow traps will be examined.

1. The weakly bonded electrons caused a Maxwell–Wagner type interfacial polarisation under the applied external field;
2. polarisation will be caused by associations of defects like ($Ti^{3+} - V_O^{\bullet}$) and/or ($V''_{Sr} - 2V_O^{\bullet}$) and the small adjustment of their relative positions under the applied external field will produce dielectric relaxation.

4.3.1 Maxwell–Wagner type polarisation

The high value of the permittivity of the second set of peaks (for $x = 0{\cdot}0133$, about 7000 at 1 kHz) as well as the conductivity values could suggest an interfacial polarisation of the Maxwell–Wagner type.[21] This kind of interfacial polarisation was usually adopted to explain the experimental results in $SrTiO_3$ based materials used as boundary layer capacitors, with extremely high permittivity.[12,22,23] Interfacial polarisation occurring between two different conducting areas could be originated if the monophasic samples had an inhomogeneous microstructure. This type of microstructure could be originated by the lost of oxygen from the bulk of the grains [eqn (7a) and (7b)] during the high temperature sintering followed by a re-oxidation of a surface layer at the grain boundaries during the cooling down process. A microstructure consisting of high conductive grains and low conductive grain boundaries was then formed and interfacial polarisation will occur.

If this was so, the presence of the second set of peaks in the as-sintered samples, and the disappearance of the peaks after annealing in O_2 could then be explained. However, it is difficult to explain why higher peaks were obtained after the sample was annealed in N_2 at 1000°C for 88 h [cf. Figure 2(a) and (c)], since when the samples were annealed in N_2, reduction on the surface layer which was previously oxidised during the sintering–cooling process would happen. It is therefore unlikely that an interfacial polarisation is at the origin of the second set of peaks.

It should be mentioned that before and after annealing both the lattice parameter and the grain size are the same within the experimental error and a uniform distribution of the elements (Sr, Bi, Ti) was observed by the SEM X-ray line profile analysis. Excluding grain boundary segregations not possible to observed in this way, this also supports that the second set of peaks is not likely due to interfacial polarisation.

In addition, it is doubtful that the simple Maxwell–Wagner model can provide a systematic dependence of the polarisation and relaxation parameters on the Bi concentration.

4.3.2 Dipole polarisation of associations of defects, such as ($Ti^{3+} - V_O^{\bullet}$) or ($V''_{Sr} - 2V_O^{\bullet}$)

Based on the standpoint of the universal theory[24] for dielectric response in condensed materials, the relaxation process, characterised by a loss peak behaviour, occurs primarily in dipole-like systems. From the experimental fact (4) indicating that the activation energy for relaxation (in the range of 0·32–0·49 eV) is higher than the activation energy for electrical conduction, a dipole-like polarisation mechanism can be thought as the most probable in the present system.

Several kinds of defects, such as $Bi_{Sr}^{\bullet}$, Ti'_{Ti} (Ti^{3+}), $V_O^{\bullet}$, $V_O^{\bullet\bullet}$, and V''_{Sr}, can be considered in Bi-doped $SrTiO_3$. Because of the Coulomb forces, defects with positive charge can combine with defects with negative charge, and form dipole defect associations like ($Ti^{3+} - V_O^{\bullet}$), ($V''_{Sr} - 2V_O^{\bullet}$), ($Ti^{3+} - Bi_{Sr}^{\bullet}$), ($V''_{Sr} - 2Bi_{Sr}^{\bullet}$), ($V''_{Sr} - V_O^{\bullet}$) or ($2Ti^{3+} - V_O^{\bullet\bullet}$). In the temperature regime of the present work for the second set of peaks, $V_O^{\bullet\bullet}$ can be neglected because it has high ionisation energy.[25] Considering that the second set of peaks is intimately related with oxygen vacancies, it is reasonable to suppose that the most probable defect associations are ($Ti^{3+} - V_O^{\bullet}$) and ($V''_{Sr} - 2V_O^{\bullet}$). Consequently, a small adjustment of the positions of the components of the defect association, under an external electrical field, will contribute to the dielectric polarisation and relaxation of the second set of peaks.[24]

Based on this hypothesis, the experimental fact (1) can be explained, i.e. when the Bi content $x \leq 0{\cdot}08$, the defect structure can be described by both eqns (6) and (7). The permittivity of the material depends on the concentration of the oxygen vacancies. Because of the high sintering temperature used when the Bi content was low, a high

intrinsic oxygen vacancy concentration will develop, leading to high permittivity. As the Bi content $x \geq 0{\cdot}10$, the defect structure of the sample is mainly described by eqn (6), the oxygen vacancy concentration is small, hence, especially, in the low temperature range, the second set of peaks disappeared.

The oxygen vacancies can be filled after heat treatment in O_2 or air, and will be again created after annealing in N_2, hence changing the concentration of the dipoles and providing an explanation for the permittivity variations described by the experimental result (2).

The experimental result (3) can be rationalised since with the increase in the substitution of the Bi ions, the crystal lattice will be much distorted,[5,6,10] being then reasonable to assume that the movement of the dipoles becomes difficult, and a higher activation energy for the dielectric relaxation is needed.

5 Conclusions

Two sets of permittivity peaks were observed in $(Sr_{1-1{\cdot}5x}Bi_x)TiO_3$ ceramics for $x \leq 0{\cdot}08$. The second set of peaks situated at around 200–300 K had frequency dispersion behaviour. These peaks were shifted to higher temperatures when the Bi content in the solid solution increased, and vanished during annealing in air or oxygen but increased during annealing in nitrogen. The activation energies for relaxation are calculated to be in the range of 0·32–0·49 eV. The results indicate that the origin of these peaks are closely related to an oxidation $\leftrightarrow$ reduction process of the samples. The discussion on dielectric properties points to a possible mechanism of the dielectric polarisation and relaxation related with the small movement of $(Ti^{3+} - V_O^{\bullet})$ and/or $(V''_{Sr} - 2V_O^{\bullet})$ dipoles.

Acknowledgements

The authors would like to thank the financial supports of the Praxis XXI, JNICT, Portugal. One of the authors (A.C.) would also thank the Zhejiang University, People's Republic of China for permitting his leave and work in the University of Aveiro.

References

1. Skanavi, G. I. and Matveeva, E. N., New nonpiezoelectric dielectrics with very high dielectric permeability and small conductivity. *Sov. Phys. JETP*, 1957, **3**, 905–908.
2. Skanavi, G. I., Ksendzov, I. M., Trigubenko, V. A. and Prokhvatilov, V. G., Relaxation polarisation and losses in *non-ferroelectric* dielectrics with high dielectric constants. *Sov. Phys. JETP*, 1958, **6**, 250–259.
3. Gubkin, A. N., Kashtanova, A. M. and Skanavi, G. I., Dielectric properties of strontium bismuth titanates at low temperature. *Soviet Phys.: Solid State*, 1961, **3**, 807–813.
4. Smolenskii, G. A., Isupov, V. A., Agranovskaya, A. I. and Popov, S. N., Ferroelectrics with diffuse phase transitions. *Sov. Phys., Solid State*, 1967, **2**, 2584–2594.
5. Zhi, Y., Chen, A., Vilarinho, P. M., Mantas, P. Q. and Baptista, J. L., Dielectric relaxation behaviour of Bi:$SrTiO_3$: I, The low temperature permittivity peak. *Journal of the European Ceramic Society*, in press.
6. Zhi, Y., Chen, A., Vilarinho, P. M., Mantas, P. Q. and Baptista, J. L., in Proceedings Electroceramics V, International Conference on Electronic Materials and Applications, Vol. 1, eds J. L. Baptista, J. A. Labrimcha, P. M. Vilanimho and F. J. J. Magaeliaës, Universidade de Aveiro, Portugal, 1996, pp. 491–495.
7. Tien, T. Y. and Cross, L. E., Dielectric relaxation in strontium titanate solid solutions containing Lathania. *Jpn. J. Appl. Phys.*, 1967, **6**(3), 459–68.
8. Iguchi, E. and Lee, K. J., Dielectric relaxation in $SrTiO_3$ doped with La_2O_3 and MnO_2 at low temperatures. *J. Mat. Sci.*, 1993, **28**, 5809–5813.
9. Johnson, D. W., Cross, L. E. and Hummel, F. A., Dielectric relaxation in strontium titanates containing rare-earth ions. *J. Appl. Phys.*, 1970, **41**(7), 2828–2833.
10. Kiseleva, K. V. and Bohdanov, S. V., Investigation of the structure of $SrTiO_3$–$3Bi_2O_3$ solid solutions. *Sov. Phys. Solid State*, 1964, **5**, 2294–2296.
11. Cole, K. S. and Cole, R. H., Dispersion and absorption in dielectrics I. Alternating current characteristics. *J. Chem. Phys.*, 1941, **9**, 341–351.
12. Burn, I. and Neirman, S., Dielectric properties of donor-doped polycrystalline $SrTiO_3$. *J. Mater. Sci.*, 1982, **17**, 3510–3524.
13. Chen, A. and Zhi, Y., Dielectric properties and complex-defect structure in $(Sr_1-xBi_2x/3)TiO_3$ ceramics. *J. Appl. Phys.*, 1992, **71**, 4451–4454.
14. Zhi, Y. and Chen, A., A positron annihilation study of $SrTiO_3$-based ceramics. *J. Phys.: Condensed Matter*, 1993, **5**, 1877–1893.
15. Chan, N. H., Sharma, R. K. and Smyth, D. M., Nonstoichiometry in $SrTiO_3$. *J. Electrochem Soc. Solid-State Science and Technology*, 1981, **128**, 1762–1769.
16. Walters, L. C. and Grace, R. E., Diffusion of point defects in strontium titanate. *J. Phys. Chem. Solids*, 1967, **28**, 239–244; Formation of point defects in strontium titanate. *J. Phys. Chem. Solids*, 1967, **28**, 245–248.
17. Eror, N. G. and Balachandran, U., High-temperature defect structure of acceptor-doped strontium titanate. *J. Am. Ceram. Soc.*, 1982, **65**, 426–431.
18. Paladino, A. E., Oxidation kinetics of single-crystal $SrTiO_3$. *J. Am. Ceram. Soc.*, 1965, **48**, 476–478.
19. Schward, D. B. and Anderson, H. U., Determination of oxygen chemical diffusion coefficient in single crystal $SrTiO_3$ by capacitance manometry. *J. Electrochem. Soc.*, 1975, **122**, 707–710.
20. Eror, N. G. and Balachandran, U., Self-compensation in Lanthanum-doped strontium titanate. *J. Solid State Chemistry*, 1981, **40**, 85–91.
21. von Hippel, A.,*Dielectric and Waves*. John Wiley and Sons, New York, 1954.
22. Stumpe, R., Wagner, D. and Bauerle, D., Influence of bulk and interface properties on the electric transport in ABO_3 perovskites. *Phys. Stat. Sol. (a)*, 1983, **75**, 143–154.
23. Parkash, Om, Prasad, Ch D. and Kumar, D., Dielectric relaxation behaviour of the system $Sr_{1-x}La_xTi_{1-x}Co_xO_3$. *J. Mat. Sci.*, 1990, **25**, 487–492.
24. Jonscher, A. K., *Dielectric Relaxation in Solids*. Chelsea Dielectrics Press, London, 1983, p. 326.
25. Long, S. A. and Blumenthal, R. N., Ti-rich nonstoichiometric $BaTiO_3$: II, Analysis of defect structure. *J. Am. Ceram. Soc.*, 1971, **54**, 577–583.